J Eng Math (2016) 101:201–217
DOI 10.1007/s10665-016-9855-9

Effects of magnetic-field-dependent viscosity at onset of convection in magnetic nanofluids

M. Arora · R. Singh · M. K. Panda

Received: 25 February 2015 / Accepted: 5 March 2016 / Published online: 12 May 2016

Abstract Convective instability in a thin layer of a magnetic nanofluid heated from below is examined within the framework of linear stability theory. Recent results, in particular those of Blums et al. (J Phys 20:1–5, 2008), have shown the importance of the dependence of the thermophysical properties of magnetic nanofluids on an externally applied magnetic field while studying thermomagnetic convection in a magnetic nanofluid. The model used incorporates the effect of Brownian diffusion, thermophoresis, and magnetophoresis. In addition, we assume that the viscosity of the magnetic nanofluid is a function of the externally applied magnetic field. The resulting eigenvalue problem from the linear stability analysis is solved by employing the Chebyshev pseudospectral method, and the results are discussed for water- and ester-based magnetic nanofluids. A "tight coupling" between buoyancy and magnetic forces has been observed in magnetic nanofluids. The effects of the important parameters of the problem are examined at the onset of convection.

Keywords Magnetic field dependent viscosity · Magnetic nanofluids · Microgravity

Mathematics Subject Classification 76E06 · 76W99 · 80A20

1 Introduction

Nanofluids are usually defined as fluids in which large numbers of small ferromagnetic particles having dimension of the order of 10^{-9}m are dispersed. These particles are known as nanoparticles, and the fluid in which the particles are dispersed is called the *base fluid*. The term *nanofluid* in its present usage was apparently coined by Choi [1]. Water or any other organic solvent can be used as a base fluid [2]. The particles used in nanofluids are usually made up of metals, oxides, or carbon nanotubes. Recently, the interest in nanofluids has been revived for two reasons: first, they have become sufficiently cheap; second, large numbers of potential practical applications of nanofluids have been discovered [3]. Nanofluids possess a large number of interesting characteristic properties, and

M. Arora · R. Singh (✉)
Department of Mathematics, Central University of Himachal Pradesh, TAB, District Kangra, Shahpur, HP 176206, India
e-mail: ravinder.iit@gmail.com; ravinder@cuhimachal.ac.in

M. K. Panda
Department of Mathematics, PDPM IIITDM-Jabalpur, Dumna Airport Road, Jabalpur, MP, India
e-mail: mkpanda@iiitdmj.ac.in

principal among them are an increase in the effective thermal conductivity and heat transfer enhancement. In [4] Eastman et al. reported a 40 % increase in the effective thermal conductivity in ethylene-glycol-based nanofluids. In alumina-water-based nanofluids, an enhancement of 10–30 % effective thermal conductivity was reported in [5].

Heat transfer enhancement by nanofluids, as expected, has attracted the attention of many researchers. Motivated to find an explanation for the anomalous heat transfer enhancement observed in nanofluids, Buongiorno [3] proposed a model taking into account the effects of Brownian diffusion (random diffusion of nanoparticles in the base fluid) and thermophoresis (motion of nanoparticles induced by a temperature gradient). He then observed that the anomalous heat transfer enhancement could not be attributed solely to nanoparticle dispersion and turbulent intensity. An alternative explanation for the increase of the heat transfer coefficient proposed by Buongiorno was that a significant decrease in the viscosity results within the boundary layer owing to the temperature gradient and thermophoresis, which leads to heat transfer enhancement. The same problem for the laminar free convection of Newtonian nanofluids was studied by Polidori et al. [6]. The Nusselt number (a dimensionless heat transfer coefficient) remains higher in the turbulent regime than in the laminar regime. Thus one is led to conclude that an increase in the Nusselt number in the turbulent regime could be one possible source of heat transfer enhancement. Another possible reason for anomalous heat transfer could be that Brownian motion and thermophoresis are considered to be two fundamental reasons for the free movement of nanoparticles in the base fluid. Natural convection, therefore, seems to be another possible source of enhancement of effective thermal conductivity because of the free movement of nanoparticles in base fluid [3,7].

Most nanofluid properties are volume-fraction dependent (e.g., thermal conductivity). In [7] Tzou studied the critical Rayleigh number, which separates the laminar regime from the turbulent regime, for the onset of Rayleigh–Bénard instability in nanofluids, assuming the nanofluid properties are not dependent on the volume fraction of nanoparticles. In the absence of such a dependence, he reported a significant reduction in the critical Rayleigh number and thus the "dominance of turbulence." The collective effect of Brownian motion and thermophoresis was shown to advance the onset of convection. Since the Nusselt number can be higher than that in laminar flows, the overall heat transfer rate can be higher in a turbulent regime than that in a regular laminar fluid. Using a Galerkin method, Dhananjay et al. [8] studied Rayleigh–Bénard convection in nanofluids when both boundaries are free. They also addressed the oscillatory case that had been missed earlier by Tzou [7,9]. The onset of convection in a horizontal nanofluid layer of finite depth was studied by Nield and Kuznetsov [2]. They observed that the critical Rayleigh number decreased by a substantial amount if the basic nanoparticle distribution was top-heavy, and increased if the basic nanoparticle distribution was bottom-heavy, by the presence of nanoparticles. In the case where nanoparticles amass near the bottom of the nanofluid layer, oscillatory instability was observed to be possible. The instability of nanofluids in a shallow cavity heated from below was studied by Alloui et al. [10]. Both analytical and numerical studies were conducted. Among other things, they observed that heat transfer enhancement in nanofluids depended on the Rayleigh number and the volume fraction of the nanofluid.

Magnetic nanofluids (MNFs) are nanofluids placed in an ambient magnetic field. MNFs comprise a distinctive class of nanofluids that display both magnetic and fluid properties. This dual character of MNFs offers the prospect of controlling their flow and heat transfer properties via an externally applied magnetic field [11]. MNFs find applications in fields such as liquid seals in rotatory shafts for vacuum systems, hard-disk devices of personal computers, and the cooling and damping of loudspeakers, to name few.

The magnetic susceptibility of MNFs is a function of temperature; thus, the temperature gradient induces spatial gradients in magnetic susceptibility. Convection induced by these two gradients is known as thermomagnetic convection [11]. Finlayson [12] studied the instability in a ferrofluid layer heated from below. The linear stability problem was solved for shear–free and rigid–rigid boundaries. The results predicted that convection could also be driven by the magnetic forces alone, in the absence of gravity. Using a Galerkin method Gotoh and Yamada [13] investigated the linear instability in a horizontal magnetic fluid layer confined between two ferromagnetic boundaries and heated from below in an ambient vertical magnetic field. They obtained a relation between the critical Rayleigh number Ra_c and magnetic number N, from which they deduced that Ra_c decreases as N increases. They further concluded that the effects of magnetic force and buoyancy compensate each other. For more on the convective instability problem and related heat transfer aspects, see [14–16] and references therein.

The problem of analyzing the instability of MNFs has been studied less extensively than the analogous problem of nanofluid convection. Using nonlinear stability analysis, Sunil and Mahajan [17] analyzed instability in a ferrofluid layer heated from below. Mahajan and Arora [18] investigated the effects of rotation at the onset of convection in a thin layer of a MNF using linear theory. The model used by them incorporated the effects of Brownian diffusion, thermophoresis, and magnetophoresis. They observed that magnetic forces dominate the buoyancy force in 1 mm thick fluid layers. For more studies related to thermomagnetic convection in MNF, the reader is referred to [19–22].

The heat transfer intensity of MNFs is characterized by the Rayleigh number Ra, which is the sum of thermomagnetic and thermogravitational parts, $\mathrm{Ra} = \mathrm{Ra_m} + \mathrm{Ra_T}$. Thus the intensity of thermomagnetic convection in general and the efficiency of devices made from MNFs in particular depend not only on magnetic and temperature field distributions but also on the thermophysical properties of MNFs and the extent of the dependence of magnetization on temperature [11]. Some previous works ignored the effects of a magnetic field on the thermophysical properties of MNFs. Recent studies have highlighted this dependence. The results of the study by Blum et al. [19] have confirmed the so-called additive action of thermogravitation and thermomagnetic forces on the heat transfer capacity of ferrofluids. Thus it is important to take into account the dependence of thermophysical properties of MNFs on externally applied magnetic fields while studying thermomagnetic convection in MNFs.

In this work, the effects of magnetic-field-dependent (MFD) viscosity on the onset of convection in MNFs are studied using linear stability theory. The Chebyshev pseudospectral method is used to solve the eigenvalue problem in gravity as well as in a microgravity environment for water- and ester-based MNFs.

2 Formulation

We consider an infinite horizontal layer of an incompressible MNF having a variable viscosity $\mu_1 = \mu(1 + \boldsymbol{\delta} \cdot \boldsymbol{B})$ and heated from below. Here μ_1 is the MFD viscosity, μ is the viscosity of the fluid in the absence of an applied magnetic field, $\boldsymbol{B}$ is the magnetic induction, and $\boldsymbol{\delta} = \delta_1\mathbf{i} + \delta_2\mathbf{j} + \delta_3\mathbf{k}$ is the variation coefficient of viscosity, which we assume to be isotropic, i.e., $\delta_1 = \delta_2 = \delta_3 = \delta$. The fluid is assumed to occupy the layer $z \in [0, d]$, with gravity, g, acting in the negative z-direction. The magnetic field $\boldsymbol{H} = H_0^{\mathrm{ext}}\boldsymbol{k}$ acts outside the layer (Fig. 1).

The MNF is assumed to be incompressible, so the equation of continuity gives

$$\nabla \cdot \boldsymbol{u} = 0, \tag{1}$$

where $\boldsymbol{u}$ is the MNF velocity.

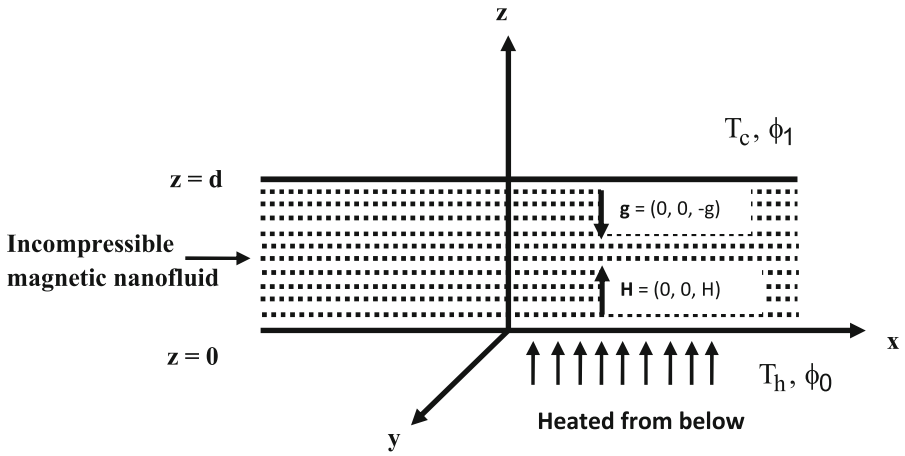

Fig. 1 Geometric configuration of problem

Following [3,12], the equation of momentum, under the Boussinesq approximation, is given by the following equation

$$\rho_f \left(\frac{\partial \boldsymbol{u}}{\partial t} + \boldsymbol{u} \cdot \nabla \boldsymbol{u} \right) = -\nabla p + \mu_1 \nabla^2 \boldsymbol{u} + \mu_0 (\boldsymbol{M} \cdot \nabla) \boldsymbol{H} - \rho g \boldsymbol{k}, \tag{2}$$

where $\rho_f, t, p, \boldsymbol{M}, \mu_0$, and ϕ are the fluid density, time, pressure, magnetization, magnetic permeability of the vacuum, and nanoparticle volume fraction, respectively. Here ρ is the total density of the nanofluid, which we assume to be given by

$$\rho = \rho_p \phi + \rho_f (1 - \phi)\{1 - \alpha (T - T_c)\},$$

where ρ_p is the nanoparticle density, $T - T_c$ is the temperature difference, and α is the coefficient of thermal expansion.

When thermophoresis is taken into account, the conservation equation for the MNF, in the absence of chemical reactions, takes the form [3,23]

$$\frac{\partial \phi}{\partial t} + \boldsymbol{u} \cdot \nabla \phi = -\frac{1}{\rho_p} \nabla \cdot \boldsymbol{j}_p, \tag{3}$$

where $\boldsymbol{j}_p$ is the mass flux for the MNF, given by the sum of "diffusiophoresis," thermophoresis, and "magnetophoresis" as

$$\boldsymbol{j}_p = \boldsymbol{j}_{pB} + \boldsymbol{j}_{pT} + \boldsymbol{j}_{pM} = -\rho_p D_B \nabla \phi - \rho_p D_T \frac{\nabla T}{T} + \rho_p D_H \nabla H, \tag{4}$$

where D_B is the Brownian diffusion coefficient, D_T is the thermophoretic diffusion coefficient, and D_H is the magnetophoretic diffusion coefficient. Using Eq. (4), the conservation equation for MNF (3) becomes

$$\frac{\partial \phi}{\partial t} + \boldsymbol{u} \cdot \nabla \phi = \nabla \cdot \left(D_B \nabla \phi + D_T \frac{\nabla T}{T} - D_H \nabla H \right). \tag{5}$$

The thermal energy equation for the MNF can be written

$$(\rho c)_f \left(\frac{\partial T}{\partial t} + \boldsymbol{u} \cdot \nabla T \right) = -\nabla \cdot \boldsymbol{V} + h_p \nabla \cdot \boldsymbol{j}_p, \tag{6}$$

where c_f is the MNF specific heat, T is the MNF temperature, h_p is the specific enthalpy of the MNF material, and $\boldsymbol{V}$ is the energy flux with respect to a frame moving with the MNF velocity $\boldsymbol{u}$, is given by the following equation

$$\boldsymbol{V} = -k_1 \nabla T + h_p \boldsymbol{j}_p.$$

Here k_1 is the MNF thermal conductivity. Substituting the preceding expression for $\boldsymbol{V}$ into Eq. (6) and using the vector identity $\nabla h_p = c_p \nabla T$, we get

$$(\rho c)_f \left(\frac{\partial T}{\partial t} + \boldsymbol{u} \cdot \nabla T \right) = \nabla \cdot (k_1 \nabla T) + \rho_p c_p \left(D_B \nabla T \cdot \nabla \phi + D_T \frac{\nabla T \cdot \nabla T}{T} - D_H \nabla T \cdot \nabla H \right), \tag{7}$$

where c_p is the specific heat of the nanoparticle material.

Maxwell's equations in the magnetostatic limit are

$$\nabla \cdot \boldsymbol{B} = 0, \quad \nabla \times \boldsymbol{H} = 0, \quad \boldsymbol{B} = \mu_0(\boldsymbol{M} + \boldsymbol{H}). \tag{8}$$

In general, magnetization is a function of the magnetic field, particle concentration, and temperature. At equilibrium, it is aligned with the stationary magnetic field. It is assumed to be governed by Langevin's formula [24]:

$$\boldsymbol{M}_{eq} = \frac{\boldsymbol{H}}{H} M_s \phi L(\alpha_L) = \frac{\boldsymbol{H}}{H} M_{eq}(H, \phi, T), \tag{9}$$

where

$$L(\alpha_L) = \coth(\alpha_L) - \frac{1}{\alpha_L}, \qquad \alpha_L = \frac{mH}{k_B T},$$

where k_B is Boltzmann's constant and M_s is the magnetic saturation.

To obtain the steady-state solution, following [12], we first linearize the magnetization equation M_{eq} as follows:

$$M_{eq}(H, \phi, T) = M_0 + \chi(H - H_0) - K_m(T - T_h) + K_p(\phi - \phi_0),$$

where χ is the tangent magnetic susceptibility, and K_m and K_p are the magnetic coefficients. The tangent and chord magnetic susceptibility χ, χ_2 can be estimated by Langevin's formula (9) for a different Langevin parameter α_L [25]:

$$\alpha_L = \frac{mH_0}{k_B T_h} = \begin{cases} \ll 1, & \chi = \frac{M_S m}{3k_B T_h}, \quad \chi_2 = \chi, \\ \simeq 1, & \chi = \frac{M_S m}{k_B T_h} L'(\alpha_L), \quad \chi_2 = \frac{M_S}{T_h} L(\alpha_L), \\ \gg 1, & \chi = \frac{M_S k_B T_h}{m H_0^2}, \quad \chi_2 = \frac{M_S}{H_0}\left(1 - \frac{1}{\alpha_L}\right). \end{cases}$$

We assume that the temperature and the volumetric fraction of the particles are constant at the boundaries. Thus the boundary conditions are

$$\left.\begin{array}{l} w = 0, \quad T = T_h, \quad \phi = \phi_0 \quad \text{at} \quad z = 0, \\ w = 0, \quad T = T_c, \quad \phi = \phi_1 \quad \text{at} \quad z = d, \end{array}\right\} \tag{10}$$

with $\partial w/\partial z = 0$ on a rigid surface and $\partial^2 w/\partial z^2 = 0$ on a stress-free surface. We also assume that the normal component of magnetic induction and the tangential component of the magnetic field are continuous across the boundary.

Equations (1)–(9) are made dimensionless by scaling all lengths with d, time with d^2/κ, pressure with $\mu\kappa/d^2$, velocity with κ/d, temperature with $T_h - T_c$, concentration with $\phi_0 - \phi_1$, H with H_0, and M with M_0. Here, $\kappa = k_1/(\rho C)_f$. Then Eqs. (1)–(9) take the form

$$\nabla \cdot \boldsymbol{u} = 0, \tag{11}$$

$$\frac{1}{\mathrm{Pr}}\left(\frac{\partial \boldsymbol{u}}{\partial t} + \boldsymbol{u} \cdot \nabla \boldsymbol{u}\right) = -\nabla p + \nabla^2 \boldsymbol{u} + \{c_1(\boldsymbol{\delta} \cdot \boldsymbol{M}) + c_2(\boldsymbol{\delta} \cdot \boldsymbol{H})\}\nabla^2 \boldsymbol{u} + c_3(\boldsymbol{M} \cdot \nabla)\boldsymbol{H} - \mathrm{Rn}\ \phi \boldsymbol{k} + \mathrm{Ra}\, T \boldsymbol{k} - \mathrm{Ra}_N N_\phi T \phi \boldsymbol{k} - \rho_1 \boldsymbol{k} + \rho_2 \phi \boldsymbol{k}, \tag{12}$$

$$\frac{\partial \phi}{\partial t} + \boldsymbol{u} \cdot \nabla \phi = \frac{1}{\mathrm{Le}} \nabla^2 \phi + \frac{N_\mathrm{A}}{\mathrm{Le}} \nabla^2 T - \frac{N'_\mathrm{A}}{\mathrm{Le}} \nabla^2 H, \tag{13}$$

$$\frac{\partial T}{\partial t} + \boldsymbol{u} \cdot \nabla T = \nabla^2 T + \frac{N_\mathrm{B}}{\mathrm{Le}}(\nabla \phi \cdot \nabla T) + \frac{N_\mathrm{A} N_\mathrm{B}}{\mathrm{Le}}(\nabla T \cdot \nabla T) - \frac{N'_\mathrm{A} N_\mathrm{B}}{\mathrm{Le}}(\nabla H \cdot \nabla T), \tag{14}$$

$$\chi_2 \nabla \cdot \boldsymbol{M} + \nabla \cdot \boldsymbol{H} = 0, \tag{15}$$

$$\boldsymbol{M} = \frac{\boldsymbol{H}}{H} \frac{(1 + \chi)}{\chi_2} \left\{ \frac{\chi}{1 + \chi} H - \frac{M_1}{M_3} T + \frac{M'_1}{M'_3} \phi + c_4 \right\}, \tag{16}$$

where

$$c_1 = \mu_0 M_0, \quad c_2 = \mu_0 H_0, \quad c_3 = \frac{\mu_0 M_0 H_0 d^2}{\kappa \mu}, \quad \rho_1 = \frac{d^3 \rho_f}{\kappa \mu}(1 + \alpha T_c)g,$$
$$\chi_2 = \frac{M_0}{H_0}, \quad c_4 = \frac{M_0 - \chi H_0 + K_m T_h - K_p \phi_0}{H_0(1+\chi)}, \quad \rho_2 = \frac{d^3 \rho_f}{\kappa \mu}(\phi_0 - \phi_1)\alpha T_c g.$$

$K_m = \chi H_0/T_h$ is in general a function of the magnetic field and temperature and $K_p = \chi H_0/\phi_0$ is a function of the magnetic field and particle concentration. Here, the following are the nondimensional parameters:

$$\mathrm{Le} = \frac{\kappa}{D_B}, \quad \mathrm{Ra} = \frac{\rho_f g \alpha d^3 (T_h - T_c)}{\mu \kappa}, \quad N_\mathrm{A} = \frac{D_T (T_h - T_c)}{D_B T_c (\phi_0 - \phi_1)}, \quad \mathrm{Pr} = \frac{\mu}{\rho_f \kappa},$$
$$N'_\mathrm{A} = \frac{D_H H_0}{D_B(\phi_0 - \phi_1)}, \quad N_\mathrm{B} = \frac{(\rho C)_p (\phi_0 - \phi_1)}{(\rho C)_f}, \quad \mathrm{Rn} = \frac{(\rho_p - \rho_f)(\phi_0 - \phi_1) g d^3}{\mu \kappa},$$
$$\mathrm{Ra}_N = (1 - \phi_0)\mathrm{Ra}, \quad N_\phi = \frac{\phi_0 - \phi_1}{1 - \phi_0}, \quad M_1 = \frac{\mu_0 \chi^2 H_0^2 (T_h - T_c)}{\rho_f g \alpha d (1+\chi) T_h^2},$$
$$M_3 = \frac{\mu_0 \chi H_0^2}{\rho_f g \alpha d T_h}, \quad M'_3 = \frac{\mu_0 \chi H_0^2}{\rho_f g \alpha d \phi_0}, \quad M'_1 = \frac{\mu_0 \chi^2 H_0^2 (\phi_0 - \phi_1)}{\rho_f g \alpha d (1+\chi) \phi_0^2},$$

where Le is the Lewis number, Ra is the thermal Rayleigh number, N_A and N'_A are the modified diffusivity ratios, Pr is the Prandtl number, N_B is a modified particle-density increment, Rn is the nanoparticle Rayleigh number, and M_1, M'_1, M_3, and M'_3 are the magnetic parameters. The boundary conditions now become

$$\left.\begin{aligned} w = 0, \quad T = \frac{T_h}{T_h - T_c}, \quad \phi = \frac{\phi_0}{\phi_0 - \phi_1} \quad \text{at} \quad z = 0 \\ w = 0, \quad T = \frac{T_c}{T_h - T_c}, \quad \phi = \frac{\phi_1}{\phi_0 - \phi_1} \quad \text{at} \quad z = 1 \end{aligned}\right\}. \tag{17}$$

3 Steady-state solution

Equations (11)–(16) possess a steady-state solution in which

$$\begin{aligned} &\boldsymbol{u}_b = \boldsymbol{0}, \qquad p = p_b(z), \qquad T = T_b(z), \\ &\boldsymbol{M} = \boldsymbol{M}_b(z), \quad \phi = \phi_b(z), \quad \boldsymbol{H} = \boldsymbol{H}_b(z). \end{aligned} \tag{18}$$

Equations (11)–(16) then reduce to

$$-\frac{\mathrm{d}p_b}{\mathrm{d}z} + c_3 M_b \frac{\mathrm{d}H_b}{\mathrm{d}z} - \mathrm{Rn}\ \phi_b + \mathrm{Ra}\ T_b - \mathrm{Ra}_N\ N_\phi T_b \phi_b - \rho_1 + \rho_2 \phi_b = 0, \tag{19}$$
$$\frac{\mathrm{d}^2 \phi_b}{\mathrm{d}z^2} + N_\mathrm{A} \frac{\mathrm{d}^2 T_b}{\mathrm{d}z^2} - N'_\mathrm{A} \frac{\mathrm{d}^2 H_b}{\mathrm{d}z^2} = 0, \tag{20}$$
$$\frac{\mathrm{d}^2 T_b}{\mathrm{d}z^2} + \frac{\mathrm{d}T_b}{\mathrm{d}z}\left\{\frac{N_\mathrm{B}}{\mathrm{Le}}\frac{\mathrm{d}\phi_b}{\mathrm{d}z} + \frac{N_\mathrm{A} N_\mathrm{B}}{\mathrm{Le}}\frac{\mathrm{d}T_b}{\mathrm{d}z} - \frac{N'_\mathrm{A} N_\mathrm{B}}{\mathrm{Le}}\frac{\mathrm{d}H_b}{\mathrm{d}z}\right\} = 0, \tag{21}$$
$$\chi_2 \frac{\mathrm{d}M_b}{\mathrm{d}z} + \frac{\mathrm{d}H_b}{\mathrm{d}z} = 0, \tag{22}$$
$$M_b = \frac{1+\chi}{\chi_2}\left\{\frac{\chi}{1+\chi} H_b - \frac{M_1}{M_3} T_b + \frac{M'_1}{M'_3}\phi_b + c_4\right\}. \tag{23}$$

Using the boundary conditions (17) and Eqs. (22), (23), Eq. (20) may be integrated to give

$$\left(1+N'_{\mathrm{A}}\frac{M'_1}{M'_3}\right)\phi_b+\left(N_{\mathrm{A}}-N'_{\mathrm{A}}\frac{M_1}{M_3}\right)T_b$$
$$=-\left\{\left(1+N'_{\mathrm{A}}\frac{M'_1}{M'_3}\right)+\left(N_{\mathrm{A}}-N'_{\mathrm{A}}\frac{M_1}{M_3}\right)\right\}z\left(1+N'_{\mathrm{A}}\frac{M'_1}{M'_3}\right)\left(\frac{\phi_0}{\phi_0-\phi_1}\right)+\left(N_{\mathrm{A}}-N'_{\mathrm{A}}\frac{M_1}{M_3}\right)\left(\frac{T_h}{T_h-T_c}\right). \quad (24)$$

Substituting the preceding value of ϕ_b into Eq. (21) and again making use of Eqs. (22) and (23) gives

$$\frac{\mathrm{d}^2T_b}{\mathrm{d}z^2}+\frac{N_{\mathrm{B}}}{\mathrm{Le}}\left\{N'_{\mathrm{A}}\frac{M_1}{M_3}-\left(1+N_{\mathrm{A}}+N'_{\mathrm{A}}\frac{M'_1}{M'_3}\right)\right\}\frac{\mathrm{d}T_b}{\mathrm{d}z}=0. \quad (25)$$

The solution of Eq. (25) satisfying Eq. (17) is

$$T_b=\frac{T_h}{T_h-T_c}-\left\{\frac{1-\mathrm{e}^{-Pz}}{1-\mathrm{e}^{-P}}\right\}, \quad (26)$$

where

$$P=\frac{N_{\mathrm{B}}}{\mathrm{Le}}\left\{N'_{\mathrm{A}}\frac{M_1}{M_3}-\left(1+N_{\mathrm{A}}+N'_{\mathrm{A}}\frac{M'_1}{M'_3}\right)\right\}.$$

According to Buongiorno [3], for a typical nanofluid, $10^2 \le \mathrm{Le} \le 10^6$, while $1 \le N_{\mathrm{A}} \le 10, N'_{\mathrm{A}} \approx 10^2$ and $N_{\mathrm{B}} \approx 10^{-3}$. The ratios M_1/M_3 and M'_1/M'_3 are $\approx 10^{-2}$ and $\approx 10^{-3}$, respectively. If one takes the preceding approximations, then the exponents in Eq. (26) are small, so following [2], to a good approximation one has

$$T_b=\frac{T_h}{T_h-T_c}-z.$$

Using this we obtain the steady-state solution of Eqs. (19)–(23):

$$\boldsymbol{u}_b=\boldsymbol{0}, \quad p=p_b(z), \quad T_b=\frac{T_h}{T_h-T_c}-z, \quad (27)$$

$$\phi_b=\frac{\phi_0}{\phi_0-\phi_1}-z, \quad H_b=1-\frac{M_1}{M_3}z+\frac{M'_1}{M'_3}z, \quad (28)$$

$$M_b=1+\frac{1}{\chi_2}\left(\frac{M_1}{M_3}\right)z-\frac{1}{\chi_2}\left(\frac{M'_1}{M'_3}\right)z. \quad (29)$$

4 Linear stability problem

We consider a small perturbation of amplitude ϵ' $(0<\epsilon'\ll 1)$ to the steady-state equation (18), so that

$$\boldsymbol{u}=\boldsymbol{u}_b+\epsilon'\boldsymbol{u}', \quad p=p_b+\epsilon' p', \quad T=T_b+\epsilon'\theta',$$
$$\boldsymbol{M}=\boldsymbol{M}_b+\epsilon'\boldsymbol{M}', \quad \phi=\phi_b+\epsilon'\phi', \quad \boldsymbol{H}=\boldsymbol{H}_b+\epsilon'\boldsymbol{H}'. \quad (30)$$

Substituting the perturbed variables into Eqs. (11)–(16) and linearizing about the steady state by collecting the $O(\epsilon')$ terms and dropping the primes gives

$$\frac{1}{\mathrm{Pr}}\frac{\partial \nabla^2 w}{\partial t} = \nabla^4 w + \delta^* \nabla^4 w - \{\mathrm{Ra} M_3 - \mathrm{Ra_s} M_3'\}(\partial \nabla_H^2 \psi/\partial z) + \left\{\mathrm{Ra} M_1 - \mathrm{Ra}\frac{M_3 M_1'}{M_3'} + \mathrm{Ra}_N(1 + N_\phi z)\right\}\nabla_H^2 \theta - \left\{\mathrm{Ra}\frac{M_3 M_1'}{M_3'} - \mathrm{Ra_s} M_1' + \mathrm{Rn} + \mathrm{Ra}_N N_\phi (1 - z)\right\}\nabla_H^2 \phi, \tag{31}$$

$$\frac{\partial \theta}{\partial t} = \nabla^2 \theta + w - \frac{N_\mathrm{B}}{\mathrm{Le}}\frac{\partial \phi}{\partial z} + \frac{N_\mathrm{B} N_\mathrm{A}'}{\mathrm{Le}}\frac{\partial^2 \psi}{\partial z^2} - \left\{\frac{N_\mathrm{B}}{\mathrm{Le}} + \frac{2 N_\mathrm{A} N_\mathrm{B}}{\mathrm{Le}} - \frac{N_\mathrm{B} N_\mathrm{A}' M_1}{\mathrm{Le} M_3} + \frac{N_\mathrm{B} N_\mathrm{A}' M_1'}{\mathrm{Le} M_3'}\right\}\frac{\partial \theta}{\partial z}, \tag{32}$$

$$\frac{\partial \phi}{\partial t} = w + \frac{1}{\mathrm{Le}}\nabla^2 \phi + \frac{N_\mathrm{A}}{\mathrm{Le}}\nabla^2 \theta - \frac{N_\mathrm{A}'}{\mathrm{Le}}\frac{\nabla^2 \partial \psi}{\partial z}, \tag{33}$$

$$\frac{\partial^2 \psi}{\partial z^2} = -\frac{(1 + \chi_2)}{(1 + \chi)}\nabla_H^2 \psi + \frac{M_1}{M_3}\frac{\partial \theta}{\partial z} - \frac{M_1'}{M_3'}\frac{\partial \phi}{\partial z}, \tag{34}$$

where

$$\nabla_H^2 = \frac{\partial^2}{\partial x^2} + \frac{\partial^2}{\partial y^2}, \quad \delta^* = \mu_0 \delta H_0 (1 + \chi_2), \quad \mathrm{Ng} = M_1 \mathrm{Ra}, \quad \mathrm{Ra_s} = \frac{\rho_f g \alpha d^3 (\phi_0 - \phi_1)}{\mu \kappa}.$$

Here Ng is the magnetic thermal Rayleigh number. Since $\nabla \times \boldsymbol{H} = 0$, there exists a potential function ψ such that $\boldsymbol{H} = \nabla \psi$. Here Eq. (31) was obtained by taking the vertical component of the double curl of the linearized momentum equation.

Equations (31)–(34) comprise a boundary value problem that will be solved by the Chebyshev pseudospectral–QZ method. To apply the Chebyshev pseudospectral–QZ method to the preceding boundary value problem, we transform the present domain from [0, 1] to [−1, 1] with the coordinate transformation z to $2z$–1 in the equations. We assume that the variables $w,\ \theta,\ \phi, \psi$ have the form

$$[w, \theta, \phi, \psi] = [w(z), \theta(z), \phi(z), \psi(z)] \exp(\sigma t + \mathrm{i}(k_x x + k_y y)). \tag{35}$$

Upon substituting these equations into Eqs. (31)–(34) in the new domain, we obtain

$$\frac{\sigma}{\mathrm{Pr}}(4D^2 - k^2) w = (4D^2 - k^2)^2 w + \delta^* (4D^2 - k^2)^2 w - \left\{\mathrm{Ra} M_1 - \mathrm{Ra}\frac{M_3 M_1'}{M_3'} + \mathrm{Ra}_N \left\{1 + N_\phi \left(\frac{z + 1}{2}\right)\right\}\right\} k^2 \theta + \left\{\mathrm{Ra}\frac{M_3 M_1'}{M_3'} - \mathrm{Ra_s} M_1' + \mathrm{Rn} + \mathrm{Ra}_N N_\phi \times \left(\frac{1 - z}{2}\right)\right\} k^2 \phi + 2(\mathrm{Ra} M_3 - \mathrm{Ra_s} M_3') k^2 D\psi, \tag{36}$$

$$\sigma \theta = w + (4D^2 - k^2)\theta - 2\left\{\frac{N_\mathrm{B}}{\mathrm{Le}} + \frac{2 N_\mathrm{A} N_\mathrm{B}}{\mathrm{Le}} - \frac{N_\mathrm{B} N_\mathrm{A}' M_1}{\mathrm{Le} M_3} + \frac{N_\mathrm{B} N_\mathrm{A}' M_1'}{\mathrm{Le} M_3'}\right\} - \frac{2 N_\mathrm{B}}{\mathrm{Le}} D\phi + \frac{4 N_\mathrm{B} N_\mathrm{A}'}{\mathrm{Le}} D^2 \psi, \tag{37}$$

$$\sigma \phi = w + \frac{1}{\mathrm{Le}}(4D^2 - k^2)\phi + \frac{N_\mathrm{A}}{\mathrm{Le}}(4D^2 - k^2)\theta - \frac{2 N_\mathrm{A}'}{\mathrm{Le}}(4D^2 - k^2) D\psi, \tag{38}$$

$$4D^2 \psi = \frac{k^2 (1 + \chi_2)}{(1 + \chi)}\psi + \frac{2 M_1}{M_3} D\theta - \frac{2 M_1'}{M_3'} D\phi, \tag{39}$$

with the boundary conditions

$$\left.\begin{array}{l} w = 0, \quad \theta = 0, \quad \phi = 0 \quad \text{at} \quad z = \pm 1 \\ Dw = 0, \quad 2(1 + \chi) D\psi - k\psi = 0 \quad \text{at} \quad z = -1 \\ D^2 w = 0, \quad 2(1 + \chi) D\psi + k\psi = 0 \quad \text{at} \quad z = 1 \end{array}\right\}. \tag{40}$$

Table 1 Values of physical quantities used [25,27]

Physical properties of water- and ester-based MNFs (at $T = 298$ K)						
Base fluid	Density ρ_f (kg/m^3)	Viscosity μ (kg/m s)	Thermal conductivity k_1 (W/m K)	Magnetic saturation Ms (A/m)	Thermal expansion coefficient α (K^{-1})	Heat capacity (J/kg K)
Water	1180	0.007	0.59	15,900	5.2×10^{-4}	3545.76
Ester	1150	0.014	0.31	15,900	8.1×10^{-4}	3238.26

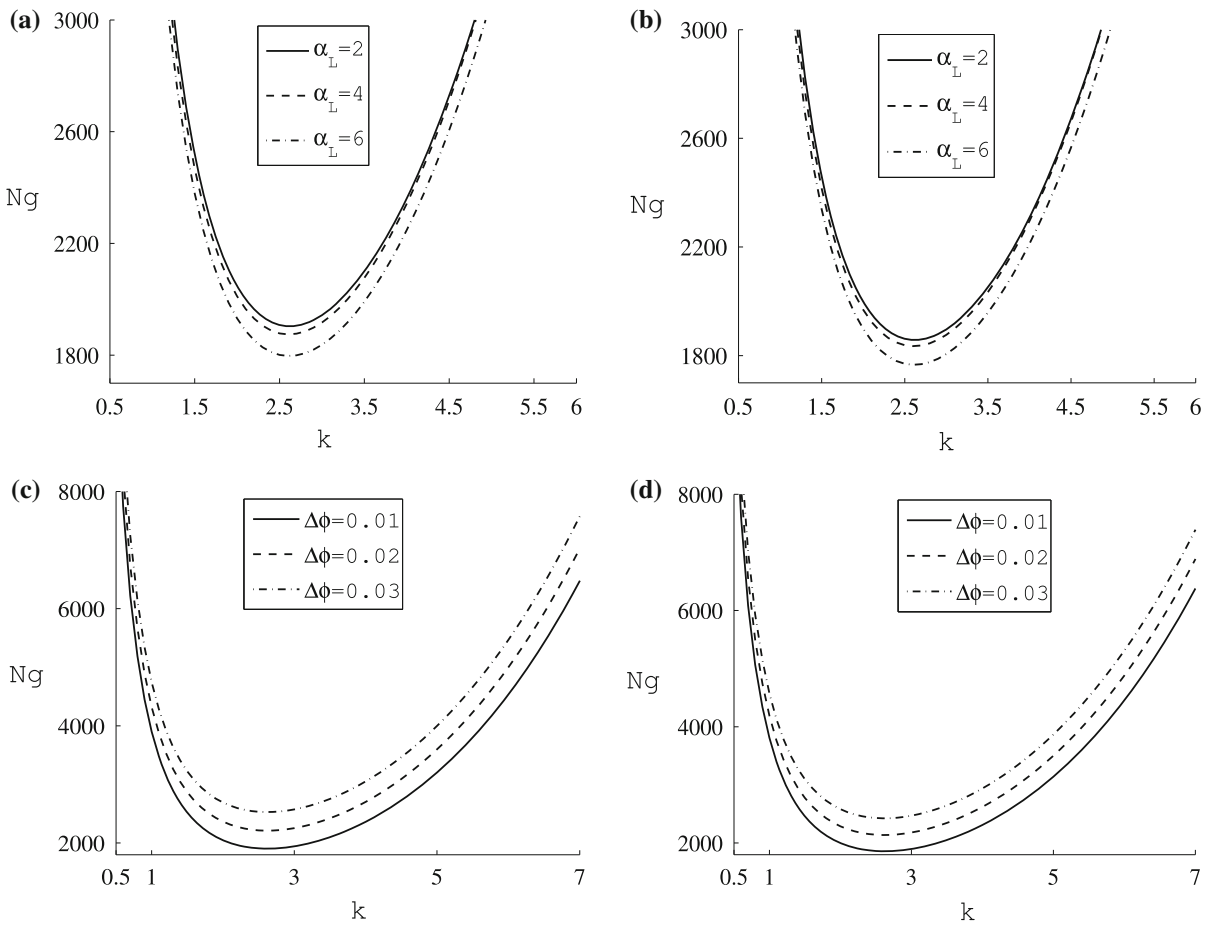

Fig. 2 **a**, **b** Neutral curves for different values of Langevin parameter α_L; **c**, **d** neutral curves for different values of volumetric fraction $\Delta\phi$ of nanoparticles. Here **a** and **c** correspond to water-based MNFs and **b** and **d** to ester-based MNFs. The fixed parameter values are $\delta = 0.01$, $\Delta\phi = 0.01$, $N_A = 10$, Le $= 200$, and $d = 0.001$

5 Method of solution

The system of equations (36)–(39) with boundary conditions (40) comprise an eigenvalue problem. The Chebyshev pseudospectral method [26] is applied to solve this eigenvalue problem. We closely follow the algorithm of Kaloni and Lou [27]. The algorithm is as follows. For a given temperature gradient β, H_0, and other physical parameters, fix $k = \sqrt{k_x^2 + k_y^2}$ and the initial trial estimates for the Rayleigh number Ra. Then use the QZ-algorithm, EIG function in MATLAB, to find the leading eigenvalue $\sigma = \sigma_r + \mathrm{i}\sigma_i$ for k. Here we recall that the leading eigenvalue

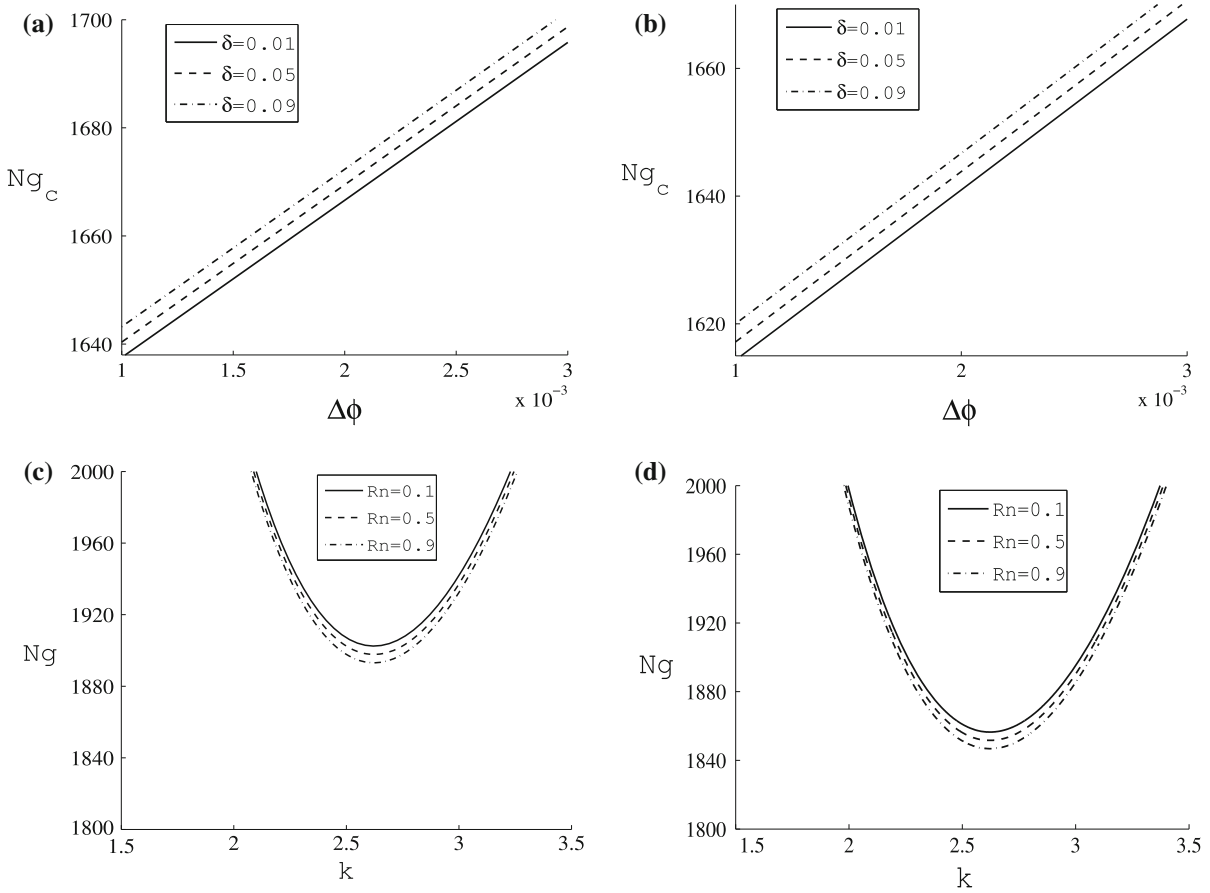

Fig. 3 **a**, **b** Variation of critical magnetic thermal Rayleigh number $\mathrm{Ng_c}$ with $\Delta\phi$; **c**, **d** neutral curves for different values of nanoparticle Rayleigh number Rn. Here **a** and **c** correspond to water-based MNFs, **b** and **d** to ester-based MNFs. The fixed parameter values are $\alpha_L = 2$, $\delta = 0.01$,$N_{\mathrm{A}} = 10$, $\mathrm{Le} = 200$, $\Delta\phi$=0.01, and $d = 0.001$

$\sigma = \sigma_r + \mathrm{i}\sigma_i$ is the one for which σ_r is the largest among the whole set of eigenvalues of the preceding eigenvalue problem. If necessary, we adjust β by the secant method to obtain β when the real part σ_r approaches zero, where σ_r is the real part of the leading eigenvalue $\sigma = \sigma_r + \mathrm{i}\sigma_i$. We repeat the preceding step until the solution with a predefined accuracy is found. The critical temperature gradient β_c with critical wave number k_c is defined as follows:

$$\beta_c = \min_k \ \beta\,(\mathrm{Pr}, \mathrm{Le}, \ldots\ldots)\,. \tag{41}$$

The function FMINBND in MATLAB was used to carry out a minimization in Eq. (41). If the imaginary part of the leading eigenvalue happens to be zero, and if σ_r approaches zero, then the instability is stationary; otherwise, it is oscillatory.

To test the accuracy of our method, we solved the Bénard problem for three types of boundary conditions, viz. rigid–rigid, rigid–free, and free–free in the absence of a magnetic field and particle concentration. The computations for the considered boundary conditions were benchmarked against Chandrasekhar's results for the Bénard problem Table III, pp. 43 [28].

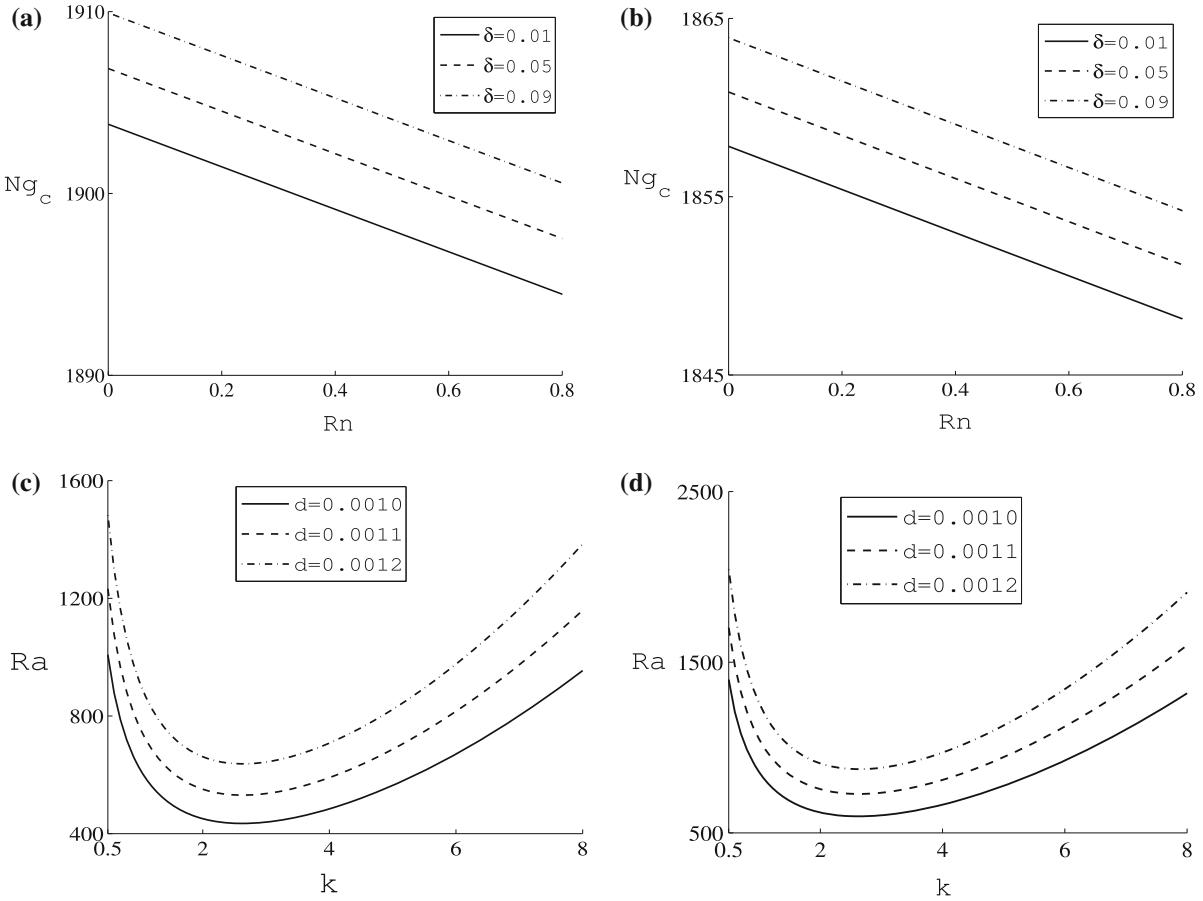

Fig. 4 **a**, **b** Variation of critical magnetic thermal Rayleigh number $\mathrm{Ng_c}$ with nanoparticle Rayleigh number Rn; **c**, **d**) neutral curves for different values of depth of nanofluid layer d. Here **a** and **c** correspond to water-based MNFs, **b** and **d** to ester-based MNFs. The fixed parameter values are $\delta = 0.01$, $N_A = 10$, Le = 200, and $d = 0.001$

6 Results

The numerical results presented in this section are for water- and ester-based MNFs. The values of the physical quantities used are taken from the table given in [25,27], which we reproduce here for the sake of completeness (Table 1).

The numerical results are provided for the nanoparticle concentration near the lower plate for a $d = 1$ mm thick layer of nanofluid. The calculations are based on 10 nm nanoparticle suspended in carrier fluid.

A neutral curve is defined as the locus of points where Re $(\sigma) = 0$. If in addition Im $(\sigma) = 0$ on such a curve, then the principle of exchange of instabilities is said to be valid.

6.1 Microgravity environment

A microgravity environment is one in which the value of acceleration due to gravity g is assumed to be negligible. In a microgravity environment we set the value of g equal to 1×10^{-6} ms^{-2}.

When a nanofluid is placed in an externally applied magnetic field in a microgravity environment, convection is driven owing to magnetic forces alone independent of the gravitational force. Owing to the temperature dependence of the magnetization of the magnetic fluid, a magnetization gradient will be established across the fluid layer.

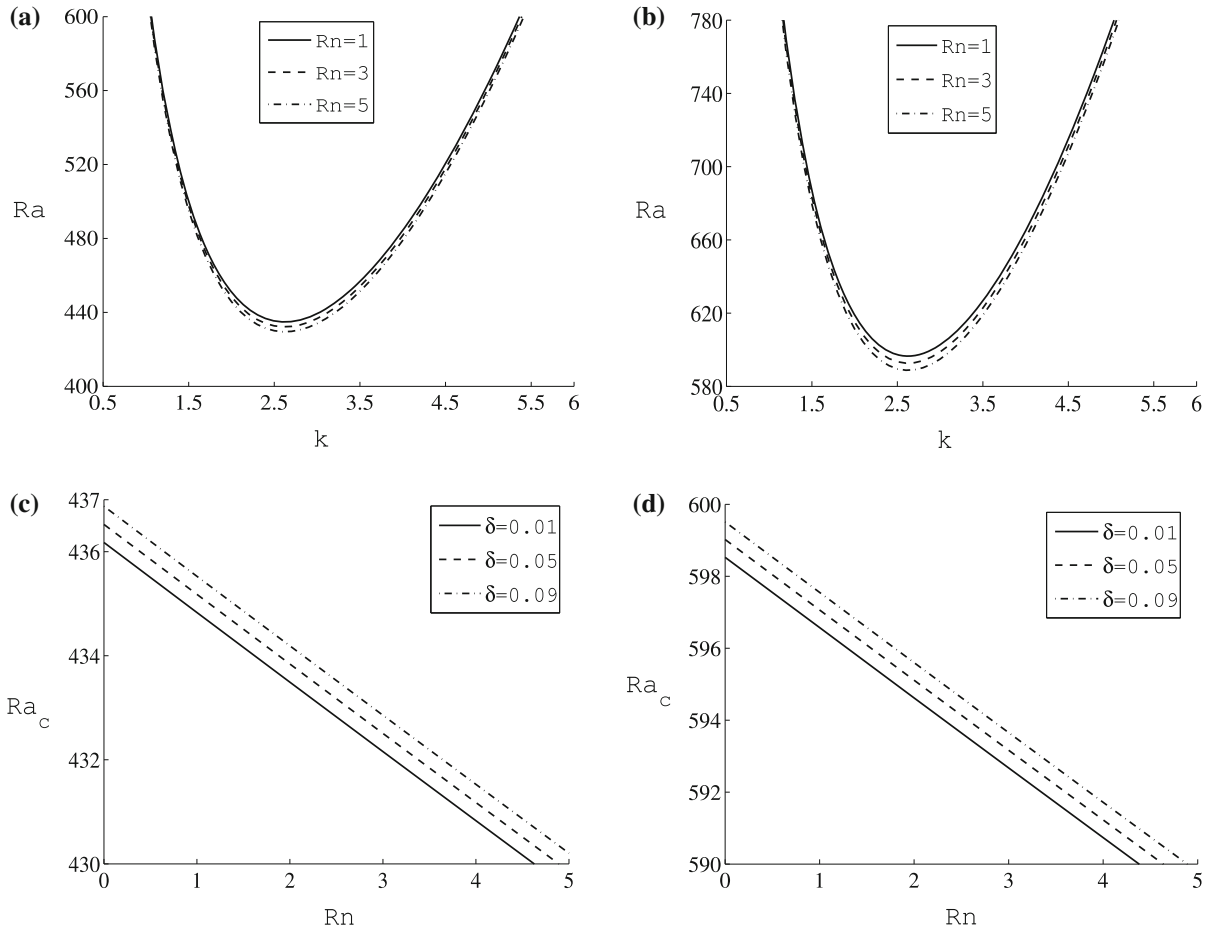

Fig. 5 **a**, **b** Neutral curves for different values of nanoparticle Rayleigh number Rn; **c**, **d** variation of critical thermal Rayleigh number $\mathrm{Ra_c}$ with nanoparticle Rayleigh number Rn. Here **a** and **c** correspond to water-based MNFs, **b** and **d** to ester-based MNFs. The fixed parameter values are $\alpha_L = 2$, $\delta = 0.01$, $N_\mathrm{A} = 10$, $\mathrm{Le} = 200$, $\Delta\phi = 0.01$, and $d = 0.001$

Magnetization of ferrofluids decreases with increasing temperature of the ferrofluid, so the direction of the magnetization gradient will be opposite to the direction of the temperature gradient. This will in turn give rise to an inner magnetic field gradient parallel to temperature gradient. A volume element displaced from the colder region with large magnetization will replace hotter ferrofluid with lower magnetization, resulting in a flow that will continue as long as the magnetic field and temperature field gradients are maintained [29].

The effects of the Langevin parameter α_L on the neutral curves for water- and ester-based MNFs are shown in Fig. 2a, b, respectively. The critical magnetic Rayleigh number $\mathrm{Ng_c}$ is finite for both types of MNF. The neutral curves show that the increase in the value of the Langevin parameter α_L decreases the critical value of the magnetic thermal Rayleigh number $\mathrm{Ng_c}$ in the microgravity environment. This is because in the microgravity environment, as the value of α_L increases, the strength of the inner magnetic field gradient ∇H also increases. The volume element moves in the fluid at greater speed, producing strong disturbances and thus resulting in a lower value of the critical magnetic thermal Rayleigh number. Since the critical magnetic thermal Rayleigh number separates the turbulent regime from the laminar regime, the heat transfer coefficient remains higher in the turbulent regime than in the laminar regime [7]. Thus the effect of increase in the magnetic field strength in the microgravity environment is to enhance the heat transfer in the water- and ester-based MNFs. Figure 2c, d shows the effects of the volumetric fraction $\Delta\phi$ of the nanoparticles on the neutral curves for both types of MNF. The critical magnetic thermal Rayleigh number

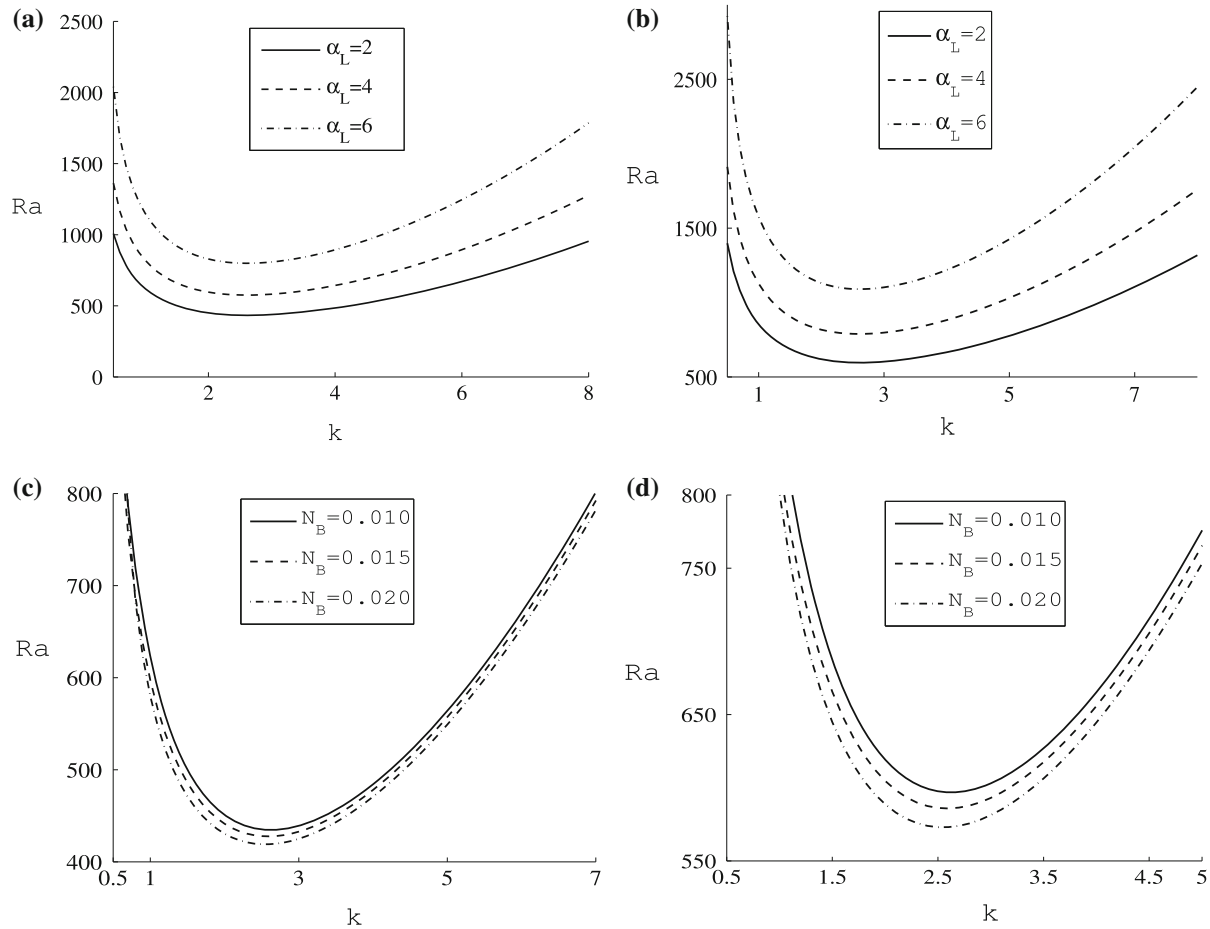

Fig. 6 **a**, **b** Neutral curves for different values of Langevin parameter α_L; **c**, **d** neutral curves for different values of modified particle density increment N_B. Here **a** and **c** correspond to water-based MNFs, **b** and **d** to ester-based MNFs. The fixed parameter values are $\alpha_L = 2$, $\delta = 0.01$, $N_A = 10$, Le $= 200$, $\Delta\phi = 0.01$, and $d = 0.001$

Ng_c increases as the value of $\Delta\phi$ increases. The temperature gradient produces an unstable, top-heavy configuration. As the particle concentration near the bottom of the fluid layer increases, the density distribution decreases with height; this has a stabilizing effect for natural convection in MNFs, which results in higher values of the critical magnetic thermal Rayleigh number. Thus increasing the value of the volumetric fraction $\Delta\phi$ of nanoparticles has a stabilizing effect on the system.

Figure 3a, b shows the variation of the critical magnetic thermal Rayleigh number Ng_c with $\Delta\phi$ at different values of the parameter δ. The figure clearly shows that Ng_c increases as $\Delta\phi$ increases.

Figure 3c, d shows that the critical magnetic thermal Rayleigh number decreases as the value of the nanoparticle Rayleigh number Rn increases. Therefore, Rn has a destabilizing effect on the system. This is because as the value of Rn increases, the Brownian motion of the nanoparticles is promoted, which in turn facilitates the development of turbulence, leading to a lower value of Ng_c. It is also worth noting that water-based MNFs are more resilient to convection than ester-based MNFs.

Figure 4a, b shows the variation of the critical magnetic thermal Rayleigh number Ng_c with the nanoparticle Rayleigh number Rn; as mentioned earlier, both of these panels clearly show that Ng_c decreases as the value of Rn increases. Since $\mu_1 = \mu(1 + \boldsymbol{\delta} \cdot \boldsymbol{B})$, at the higher value of δ, the nanoparticles in the fluid slow down owing to the high viscosity. This is manifested in the higher value of the critical magnetic thermal Rayleigh number Ng_c.

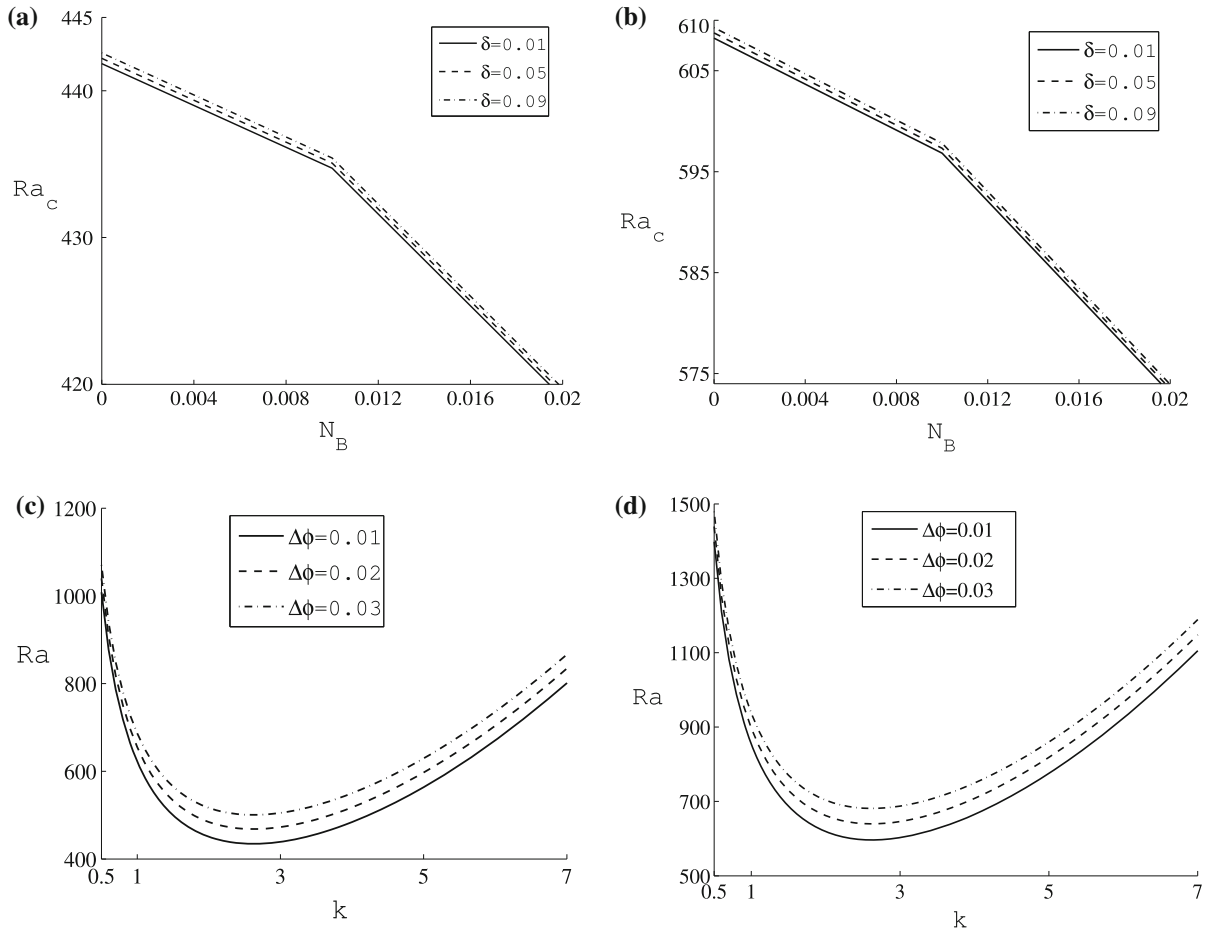

Fig. 7 **a**, **b** Variation of critical thermal Rayleigh number Ra_c for different values of modified particle density increment N_B; **c**, **d** neutral curves for different values of $\Delta\phi$. Here **a** and **c** correspond to water-based MNFs, **b** and **d** to ester-based MNFs. The fixed parameter values are $\alpha_L = 2$, $\delta = 0.01$, $N_A = 10$, Le $= 200$, $\Delta\phi = 0.01$, and $d = 0.001$

6.2 Gravity environment

The neutral curves associated with different values of d, the depth of the nanofluid layer, in a gravitational environment are plotted in Fig. 4c, d. The figure shows that the critical thermal Rayleigh number Ra_c increases as the value of d increases for both types of MNF. Since now both gravitational and magnetic forces are operational, as the depth of the nanofluid layer increases, the buoyancy force dominates the magnetic forces, which results in a higher value of Ra_c.

Figure 5a, b shows the effects of the nanoparticle Rayleigh number Rn on both types of MNF. The critical thermal Rayleigh number Ra_c decreases with an increasing value of Rn in water- and ester-based MNFs. Thus increasing the depth of the nanofluid layer has a stabilizing effect, while increasing the value of Rn has a destabilizing effect on the system.

Figure 6a, b shows the neutral curves for different values of α_L. The critical thermal Rayleigh number Ra_c increases with increases in the value of α_L, indicating that increasing α_L has a stabilizing effect on the system. When only magnetic forces were in operation, i.e., in the microgravity environment, the effect of α_L was to advance the onset of convection (Fig. 2a, b). Figure 6c, d shows the neutral curves associated with different values of modified particle density N_B. The effect of increasing the value of N_B is to advance the onset of convection. This is because the movement of the heavier nanoparticles in the fluid produces strong disturbances, which results in the lower

Table 2 Values of critical thermal Rayleigh number and critical wavenumber in gravitational environment for water- and ester-based MNFs

δ	α_L	Rigid–rigid				Rigid–free				Free–free			
		Water		Ester		Water		Ester		Water		Ester	
		k_c	$\mathrm{Ra_c}$	k_c	$\mathrm{Ra_c}$	k_c	$\mathrm{Ra_c}$	k_c	$\mathrm{Ra_c}$	k_c	$\mathrm{Ra_c}$	k_c	$\mathrm{Ra_c}$
0.01	1	3.12	668.96	3.12	920.54	2.64	547.34	2.64	750.99	2.16	432.86	2.16	591.31
	2	3.10	528.83	3.11	728.71	2.62	434.58	2.63	596.61	2.15	345.23	2.14	471.16
	3	3.09	586.54	3.09	807.68	2.61	481.14	2.61	660.15	2.13	381.33	2.14	520.26
	4	3.09	703.65	3.10	967.39	2.61	575.57	2.61	788.75	2.14	454.75	2.13	620.09
	5	3.10	840.77	3.10	1152.90	2.62	686.04	2.61	938.05	2.13	540.77	2.13	736.18
0.03	1	3.12	669.11	3.14	920.74	2.64	547.46	2.64	751.15	2.16	432.95	2.16	591.44
	2	3.11	529.05	3.11	729.01	2.63	434.76	2.63	596.85	2.15	345.36	2.14	471.35
	3	3.10	586.89	3.10	808.17	2.61	481.42	2.62	660.55	2.14	381.55	2.13	520.56
	4	3.10	704.20	3.10	968.15	2.61	576.01	2.61	789.36	2.12	455.08	2.13	620.57
	5	3.11	841.58	3.10	1154.00	2.62	686.68	2.61	938.94	2.13	541.26	2.13	736.88
0.05	1	3.12	669.26	3.13	920.94	2.64	547.58	2.64	751.32	2.16	433.04	2.16	591.57
	2	3.10	529.26	3.11	729.32	2.62	434.93	2.62	597.10	2.14	345.49	2.14	471.54
	3	3.10	587.24	3.10	808.66	2.61	481.70	2.61	660.94	2.14	381.76	2.13	520.87
	4	3.09	704.75	3.10	968.91	2.61	576.44	2.61	789.97	2.14	455.42	2.13	621.05
	5	3.10	842.38	3.11	1155.10	2.61	687.32	2.62	939.83	2.13	541.75	2.13	737.58

The fixed parameter values are $Le = 200,\ \Delta\phi = 0.01,\ N_{\mathrm{A}} = 10, d = 0.001$

Table 3 Values of critical magnetic thermal Rayleigh number and critical wavenumber in microgravity environment for water- and ester-based MNFs

δ	α_L	Rigid–rigid				Rigid–free				Free–free			
		Water		Ester		Water		Ester		Water		Ester	
		k_c	$\mathrm{Ng_c}$	k_c	$\mathrm{Ng_c}$	k_c	$\mathrm{Ng_c}$	k_c	$\mathrm{Ng_c}$	k_c	$\mathrm{Ng_c}$	k_c	$\mathrm{Ng_c}$
0.01	1	3.12	2630.60	3.12	2594.60	2.64	1758.00	2.64	1724.80	2.16	1099.10	2.16	1072.80
	2	3.10	2822.60	3.11	2773.40	2.62	1903.70	2.63	1857.70	2.15	1200.20	2.14	1160.80
	3	3.09	2848.00	3.09	2799.80	2.61	1913.30	2.61	1868.50	2.13	1200.70	2.14	1163.00
	4	3.09	2807.60	3.10	2764.70	2.61	1874.50	2.61	1834.80	2.14	1169.10	2.13	1137.40
	5	3.10	2759.60	3.10	2721.90	2.62	1832.20	2.61	1797.40	2.13	1137.80	2.13	1111.40
0.03	1	3.12	2631.70	3.14	2595.70	2.64	1758.80	2.64	1725.60	2.16	1099.60	2.16	1073.30
	2	3.11	2825.00	3.11	2775.70	2.63	1905.20	2.63	1859.20	2.15	1201.10	2.14	1161.70
	3	3.10	2851.40	3.10	2803.20	2.61	1915.60	2.62	1870.70	2.14	1202.00	2.13	1164.40
	4	3.10	2812.00	3.10	2769.00	2.61	1877.30	2.61	1837.70	2.12	1170.80	2.13	1139.10
	5	3.11	2764.90	3.10	2727.10	2.62	1835.60	2.61	1800.80	2.13	1139.90	2.13	1113.50
0.05	1	3.12	2632.90	3.13	2596.80	2.64	1759.50	2.64	1726.30	2.16	1100.00	2.16	1073.70
	2	3.10	2827.30	3.11	2778.00	2.62	1906.70	2.62	1860.70	2.14	1202.00	2.14	1162.70
	3	3.10	2854.80	3.10	2806.60	2.61	1917.80	2.61	1872.90	2.14	1203.40	2.13	1165.70
	4	3.09	2816.30	3.10	2773.30	2.61	1880.20	2.61	1840.50	2.14	1172.60	2.13	1140.90
	5	3.10	2770.20	3.11	2732.40	2.61	1839.00	2.62	1804.20	2.13	1142.00	2.13	1115.60

The fixed parameter values are $Le = 200,\ \Delta\phi = 0.01,\ N_{\mathrm{A}} = 10,\ d = 0.001$

value of $\mathrm{Ra_c}$. Figure 7a, b shows the variation of the critical thermal Rayleigh number $\mathrm{Ra_c}$ with N_B at different values of the parameter δ. As we just mentioned, the value of the critical thermal Rayleigh number $\mathrm{Ra_c}$ decreases as the value of $\mathrm{N_B}$ increases. There is a sudden change in behavior around the point 0.010; this is because some of the nanoparticles may amass near the bottom owing to sedimentation if we keep on increasing the value of $\mathrm{N_B}$.

The effects of increasing the volumetric fraction $\Delta\phi$ of nanoparticles on neutral curves are shown in Fig. 7c, d. The critical thermal Rayleigh number $\mathrm{Ra_c}$ increases with increases in the value of $\Delta\phi$. Thus increasing the value of $\Delta\phi$ has a stabilizing effect on the system.

We have also solved the same problem for other combinations of boundary conditions, viz., when both upper and lower boundaries are rigid and when both upper and lower boundaries are free. The results for these combinations of boundary conditions are displayed in Table 2 in a gravity environment and in Table 3 in a microgravity environment. The results for these boundary conditions are qualitatively similar to the results discussed earlier; thus they are not included in the paper. Tables 2 and 3 display the critical wavenumber k_c, critical thermal Rayleigh number $\mathrm{Ra_c}$, and critical magnetic thermal Rayeligh numbers $\mathrm{Ng_c}$. Our first observation from these tables is that for any given value of the parameter δ, for a given MNF, and for a particular combination of boundary conditions, the value of the critical wavenumber k_c is the same in the gravity and microgravity environments. The value of the critical magnetic Rayleigh number $\mathrm{Ng_c}$ in a microgravity environment is larger than that of $\mathrm{Ra_c}$ in gravity environment. Thus when only magnetic forces are operational, the convection gets delayed. We observe from Table 2 that the value of the critical thermal Rayleigh number $\mathrm{Ra_c}$ first decreases as α_L increases from 1 to 2 and then starts increasing with further increases in the value of α_L. In Table 3 the value of the critical magnetic thermal Rayleigh number $\mathrm{Ng_c}$ first increases as α_L increases from 1 to 3 and then starts decreasing with further increases in the value of α_L. Similar behavior was observed in [30] for water- and ester-based ferrofluids. This seems to be analogous to tight coupling between buoyancy and magnetic forces, as pointed out by Finlayson [12]. He proposed the following formula (using his notations) in the case of ferromagnetic fluids to make precise the aforementioned coupling:

$$\frac{\mathrm{Rg_c}}{\mathrm{Rg_{0c}}} + \frac{N_\mathrm{c}}{N_{0\mathrm{c}}} = 1,$$

where $\mathrm{Rg_c}$ and N_c are critical Rayleigh numbers in gravity and microgravity environments, respectively, and $\mathrm{Rg_{0c}} = 1708$, $N_{0\mathrm{c}} = 2568.5$. In our case, it is difficult to make precise this type of tight coupling.

7 Conclusions

Linear stability theory was used to study convective instability in a thin layer of MNF. The viscosity of the MNF is assumed to be dependent on the applied magnetic field. The effects of Brownian diffusion, thermophoresis, and magnetophoresis were incorporated in the mathematical model. The resulting eigenvalue problem was solved using the Chebyshev pseudospectral method. The effects of important parameters of the problem were observed at the onset of convection in microgravity and gravity environments. We draw the following conclusions:

(i) In a microgravity environment, the effect of $\Delta\phi$ is to delay the onset of convection, while α_L and Rn advance the onset of convection.
(ii) In a gravity environment, the effect of $d, \alpha_L, \Delta\phi$ is to stabilize the system, while Rn and N_B destabilize the system.

Acknowledgments The authors are grateful to the editor and anonymous referees for their valuable comments and suggestions which have helped in better exposition of the paper. The research of Monica Arora was funded by a Ph.D. Research Fellowship from the Central University of Himachal Pradesh, TAB, Shahpur (H.P.).

References

1. Choi S (1995) Enhancing thermal conductivity of fluids with nanoparticles. In: Siginer DA, Wang HP (eds) Developments and applications of non-Newtonian flows, FED vol 231/MD-vol 66. ASME, San Francisco, pp 99–105

2. Nield DA, Kuznetsov AV (2010) The onset of convection in a horizontal nanofluid layer of finite depth. Eur J Mech B Fluids 29:217–223
3. Buongiorno J (2006) Convective transport in nanofluids. ASME J Heat Trans 128:240–250
4. Eastman JA, Choi SUS, Li S, Yu W, Thompson LJ (2001) Anomalously increased effective thermal conductivities of ethylene glycol-based nanofluids containing copper nanoparticles. Appl Phys Lett 78(6):718–720
5. Das SK, Putra N, Thiesen P, Roetzel W (2003) Temperature dependence of thermal conductivity enhancement for nanofluids. ASME J Heat Trans 125:567–574
6. Polidori G, Fohanno S, Nguyen CT (2007) A note on heat transfer modeling of Newtonian nanofluids in laminar free convection. Int J Therm Sci 46(8):739–744
7. Tzou DY (2008) Thermal instability of nanofluids in natural convection. Int J Heat Mass Trans 51:2967–2979
8. Dhananjay, Agrawal GS, Bhargava R (2011) Rayleigh–Bénard convection in nanofluid. Int J Appl Math Mech 7(2):61–76
9. Tzou DY (2008) Instability of nanofluids in natural convection. ASME J Heat Trans 130:1–9
10. Alloui Z, Vassseur P, Reggio M (2011) Natural convection of nanofluids in a shallow cavity heated from below. Int J Therm Sci 50:385–393
11. Nkurikiyimfura I, Wang Y, Pan Z (2013) Heat transfer enhancement by magnetic nanofluids: a review. Renew Sustain Energy Rev 21:548–561
12. Finlayson BA (1970) Convective instability in ferromagnetic fluids. J Fluid Mech 40:753–767
13. Gotoh K, Yamada M (1982) Thermal convection in a horizontal layer of magnetic fluids. J Phys Soc Jpn 51:3042–3048
14. Blennerhassett PJ, Lin F, Stiles PJ (1991) Heat transfer through strongly magnetized ferrofluids. Proc R Soc Lond Ser A 433(1887):165–177
15. Sharifi I, Shokrollahi H, Amiri S (2012) Ferrite-based magnetic nanofluids used in hyperthermia applications. J Magn Magn Mater 324(6):903–915
16. Stiles PJ, Kagan M (1990) Thermalconvective instability of a horizontal layer of ferrofluid in a strong vertical magnetic field. J Magn Magn Mater 85:196–198
17. Sunil, Mahajan A (2008) A nonlinear stability analysis for magnetized ferrofluid heated from below. Proc R Soc A 464:83–98
18. Mahajan A, Arora M (2013) Convection in rotating magnetic nanofluids. Appl Math Comput 219:6284–6296
19. Blums E, Mezulis A, Kronkalns G (2008) Magnetoconvective heat transfer from a cylinder under the influence of nonuniform magnetic field. J Phys 20:1–5
20. Shuchia S, Sakatanib K, Yamaguchi H (2005) An application of a binary mixture of magnetic fluid for heat transport devices. Proceedings of 10th international conference on magnetic fluids. J Magn Magn Mater 289:257–259
21. Yamaguchi H, Niu X-D, Zhang X-R, Keisuke Y (2009) Experimental and numerical investigation of natural convection of magnetic fluids in cubic cavity. J Magn Magn Mater 321(22):3665–3670
22. Yamaguchi H, Niu X-D, Zhang X-R, Keisuke Y (2010) Thermomagnetic natural convection of thermo-sensitive magnetic fluids in cubic cavity with heat generating object inside. J Magn Magn Mater 322(6):698–704
23. Shliomis MI (2002) Convective instability of magnetized ferrofluids: influence of magnetophoresis and Soret effect. In: Kohler W, Weigand S (eds),Thermal nonequilibrium phenomenon in fluid mixtures. Lecture Notes in Physics, vol 584. Springer, Berlin, pp 355–371
24. Shliomis MI (1972) Effective viscosity of magnetic suspensions. Sov Phys JETP 34(6):1291–1294
25. Rosensweig RE (1997) Ferrohydrodynamics. Dover Publications, Mineola
26. Canuto C, Hussaini MY, Quateroni A, Zang T (1998) Spectral methods in fluid dynamics. Springer, New York
27. Kaloni PN, Lou JX (2002) Stability of Hadley circulations in a Maxwell fluid. J Non Newton Fluid Mech 103:167–186
28. Chandrasekhar S (1981) Hydrodynamic and hydromagnetic stability. Dover, New York
29. Völker T, Blums E, Odenbach S (2007) Heat and mass transfer phenomena in magnetic fluids. GAMM Mitt 30:185–194
30. Kaloni PN, Lou JX (2004) Convective instability of magnetic fluids. Phys Rev E 70:1–12